ARTICLE

Adsorption and photocatalytic properties of NiO nanoparticles synthesized via a thermal decomposition process

Martha Ramesh[a)]
Materials Research Lab, Department of Physics, National Institute of Technology Karnataka, Surathkal, Mangalore-575 025, India

Martha Purna Chander Rao and Sambandam Anandan
Nanomaterials and Solar Energy Conversion Lab, Department of Chemistry, National Institute of Technology, Trichy-620015, India

Hosakoppa Nagaraja[b)]
Materials Research Lab, Department of Physics, National Institute of Technology Karnataka, Surathkal, Mangalore-575 025, India

NiO nanoparticles (NPs) were synthesized at different annealing temperatures via a thermal decomposition process and characterized using X-ray diffraction, scanning electron microscopy, and UV-vis spectroscopy. The NiO NPs prepared at higher annealing temperature (400 °C) were shown excellent adsorption and photocatalytic activity toward textile dyes reactive black 5 (RB-5) and methylene blue (MB). About 87.2% of RB-5 in 60 min and 70.2% of MB in 5 h was removed using NiO NPs synthesized at 400 °C. The photocatalytic degradation of MB was found to increase with an increase in the annealing temperature of the catalyst. Moreover, the kinetic study revealed that the adsorption and photocatalytic activity of NiO NPs followed the second and first-order kinetics, respectively. The enhanced performance of NiO NPs toward dye removal might be related to its optical and structural properties.

I. INTRODUCTION

Synthetic or azo dyes are extensively used in textiles industries, wherein reactive black 5 (RB-5) and methylene blue (MB) are most abundant, excellent fabric, and have a high wet fastness profile. However, these dyes readily reduce into aromatic amines due to the presence of the characteristic double bond of nitrogen (–N=N–), which are potentially hazardous. Thus, effluent released from textile industries causes not only the coloration of water but also poses a threat to aquatic life.[1,2]

To degrade or eliminate these dyes from the waste water, first dye molecules could be adsorbed on the catalyst. Therefore, based on their molecular structure, the ability of dye adsorption on the catalyst surface can be quantized before and after exposure to light. Some dyes are normally adsorbed on the catalyst even at mild conditions. Other dyes are resistant to adsorption but can contribute to photocatalysis. In such cases, light can couple a molecular dye and catalyst through their co-adsorption on the semiconducting surface, using photon as a scaffold and solid state charge mediator.

There are many physical, chemical, and biological methods for removal of dye from wastewater.[3–6] The advanced oxidation process is an alternative route for water purification. The photocatalytic process seems to be an efficient tool in the presence of light since it uses oxidizing species such as hydroxyl radicals to degrade the organic affluent. Adsorption is also a very promising technique to eliminate the contaminants due to its simplicity and effectiveness. Carbon-based materials and various metal oxides were used as adsorbents. Though they are highly reactive with the organic affluent, due to leaching of the redox metal ions from the adsorbent, they cause intermediate metal complexes, which are incapable of adsorbing organic pollutants, resulting in lower dye removal efficiency.[7–9] Many metal oxide nanoparticles (NPs), such as Fe_2O_3, TiO_2, and CO_3O_4, were used as either adsorbent or catalyst but have limitations like poor light transmittance and tendency to aggregate to form larger particles, decreasing the dispersibility and original specific surface area, which finally weaken the catalytic activity. El-Kemary et al.[10] reported that NiO NPs are much more effective catalyst or adsorbent due to their excellent durability, high photosensitivity, and high adsorptive affinity.

The principal goal of current research is not only to find an efficient and environmentally friendly material and technology for catalysis but also to develop methods

for manipulation of the catalytic activity of NPs. In certain cases, the catalytic properties are altered by the pretreatment of the catalyst. However, low-temperature pretreatments may also cause the encapsulation of the small particles, their agglomeration as well as poisoning of the adsorbents. With regards to the heat treatment of NPs, it alters the crystallite size and influences the structural and optical properties of the NPs. It is obvious that the dye removal or degradation efficiency of the catalysts depends greatly on the manipulation of band gap with an average size on the nanometer scale.[11] Hence, the improvement in the adsorption or catalytic properties of metal oxide NPs accompanied by the changes in the optical and structural properties of small particles using thermal treatment.

In this paper, we report the synthesis and characterization of NiO NPs, as an adsorbent to remove RB-5 from the aqueous solution in the absence of light and also as a photocatalyst to degrade MB in the presence of visible light. The correlation between structural, morphological, optical, adsorption, and photocatalytic properties of NiO NPs with respect to the annealing temperature has been discussed.

II. MATERIALS AND METHODS

0.2 M of sodium hydroxide and 0.1 M of nickel nitrate hexahydrate was dissolved in 100 mL of deionized water. The above mixture was stirred at room temperature for about one hour. The resultant green colored solution was centrifuged with ethanol and deionized water several times to remove the contaminants. After that, precipitates were taken into desiccators and dried at 55 °C for 12 h. A light green powder was obtained which was annealed at 200 °C, 300 °C, and 400 °C for 120 min and used for the dye removal experiment. The prepared products were characterized by using a scanning electron microscope (SEM; JEOL-SEM, JEOL Ltd., Tokyo, Japan), an X-ray diffractometer (XRD) (PANalyticalX'Pert, PANalytical, Almelo, the Netherlands), and a UV-visible spectrometer (Ocean optics 4000, Ocean Optics, Mumbai, India).

A. Adsorption and photocatalysis experiments

The adsorption study was carried out at room temperature. Typically, 100 mL of 3×10^{-5} M RB-5 dye solution was taken in a 250 mL graduated beaker. Then, 30 mg NiO sample was weighed in an analytical balance (AUW 220D, Shimadzu, Kyoto, Japan) and added to the above dye solution. Later, the solution was stirred with a magnetic stirrer. At regular time intervals, 5 mL of aliquots were taken by using a 5 mL syringe and filtered with polyvinylidene difluoride (0.45 μm) filters to remove the catalyst particles. The residual concentration of dye has been monitored by UV-visible spectroscopy.

The photocatalytic experiment was performed in a photocatalytic chamber equipped with three tungsten halogen lamps (Osram, Munich, Germany; 150 W/24 V) which emit the radiation equal to the wave length of visible light. 100 mL of 3×10^{-5} M MB dye solution containing 30 mg NiO NPs was irradiated under visible light at the different reaction time ranging up to 5 h. Prior to irradiation, the suspension was stirred in the dark for 30 min to attain adsorption/desorption equilibrium. A 5 mL syringe and Whatman PVDF membrane (Whatman, Maidstone, United Kingdom; 0.45 μm) filter were used to extract and filter the dye suspension that was taken at definite time intervals to avoid the interruption of NiO particles during absorption measurement. The concentration of the dye has been monitored by UV-visible spectroscopy.

III. RESULTS AND DISCUSSION

To evaluate the crystal properties of annealed NiO NPs, XRD was registered as shown in Fig. 1. The diffraction patterns of NiO NPs were well indexed with standard (JCPDS card No. 01-175-0269), with simple cubic structure. From XRD, the variation in peak widening is associated with crystallite size, as given in Table I.

The crystallite size increases with the increase in annealing temperature. By increasing the annealing temperature, the nuclei grow into larger nanocrystals, and hence the crystalline volume increases, suggesting good crystallinity. It is also evident that the XRD peak broadening (FWHM) becomes narrow and diffraction peaks become more intense with enhancement of temperature, signifying that the size of NiO NPs becomes larger. The various parameters are tabulated in Table I and calculated using the following equations[12]:
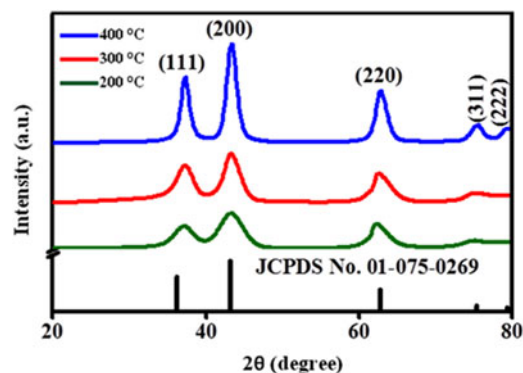

FIG. 1. XRD of the NiO NPs at different annealing temperatures (200–400 °C).

TABLE I. The optical and structural parameters of NiO NPs (where d—mean size of the crystallite, D—average particle diameter, and SA—surface area).

Temp. (°C)	d (nm)	D (nm)	SSA (nm²)	Band gap (eV)
200	2.0	2.5	79.1	3.7
300	3.1	4.2	224.7	3.2
400	5.4	7.6	742.7	2.7

$$d = \frac{0.9\lambda}{\beta \cos \theta} \quad , \qquad (1)$$

$$SSA = 6000/\rho D \quad . \qquad (2)$$

Here, d is the mean size of the crystallite (nm), λ is the wave length of Cu K$_\alpha$ radiation (0.154 nm), β is the line widening at half height of the diffraction peak (200) in radians, θ is the diffraction angle in degrees, ρ is the density of NiO 6.67 g/cm^3, D is the average particle diameter, and SSA is the specific surface area.

To study the optical properties of the prepared NiO NPs, UV-vis absorption spectra were registered as shown in Fig. 2(a). It may be noticed that the absorption edge was red-shifted with an increasing annealing temperature of the adsorbent, which is attributed to the better quantum confinement effect. The energy band gap [Fig. 2(b)] values of NiO NPs based on the optical absorption are shown in Table I. The E_g value reduces with the increase in the annealing temperature due to the increased crystallite size.[13]

To investigate the morphology of the catalyst, SEM micrographs are depicted in Fig. 3. The shape, encapsulation, size, and surface area of NiO NPs were found to mainly depend on the annealing temperature. At lower temperature, the particle growth is not thermodynamically favored, with only a few atoms can diffuse into the cluster but remaining atoms dissolve, which results in a lower particle size and surface area, as shown in Table I. The particle size of NPs was estimated using ImageJ Software (National Institute of Health, Bethesda, Maryland) of SEM images. The morphology of the adsorbent clearly shows the agglomerated shapeless particles, as shown in Fig. 3. However, at a higher temperature, a large number of atoms get activation energy and diffuse over the nucleation barrier to form clusters, resulting in particles of larger diameter and surface area. Also, the morphology of NiO NPs slowly changed to disaggregated spherical shape. The average surface area of

NiO NPs, from Eq. (2), calculated for higher annealing temperature is about 742.7 m^2/g, whereas for lower annealing temperature, it is about 79.1 m^2/g. The increased specific surface area of NPs at higher annealing temperature is due to the larger particle size.

A. Adsorption and photocatalysis

RB-5 and MB textile dyes were chosen to check the efficiency of the NiO NPs. Depending on their molecular structure, RB-5 exhibits adsorption, whereas MB exhibits photocatalytic degradation using the same catalyst. Under ambient conditions (in the absence of light and oxidants), RB-5 exhibits very strong adsorption on NiO NPs due to the strong interaction between the RB-5 and NiO. To check the effectiveness of NiO NPs toward other dyes, we chose MB dye pollutant for adsorption studies. Interestingly, only small amount of MB was adsorbed for the MB–NiO system in 6 h due to the weak interaction between the MB and NiO, as shown in Fig. 5. Thus, we further moved to find out the effective method for the removal of MB dye. It is well known that photocatalysis is an emerging technique to degrade the environment pollutants. However, the significant amount of MB was degraded by exposure of MB and NiO suspension to visible light irradiation due to the generation of highly reactive $\cdot$OH radicals, which act as strong oxidants.[14,15]

As can be seen in Fig. 4, the UV-visible spectrum recorded during the adsorption of RB-5 exhibits the peaks at 313.6 nm and 601 nm, and MB exhibits the peaks at 292 nm and 664 nm, respectively, due to various groups and structural units in the dye molecules. The peaks of both dyes in the UV region were attributed to the absorption of the π–π* transition associated with the benzene ring and naphthalene ring, while the peaks in the visible region were attributed to the absorption of the n–π* transition related to the –N=N– group in the dye molecule. The lower rate in the ultraviolet band region is ascribed to the partial removal of dye molecules due to the high energy band between the aromatic rings.[16]
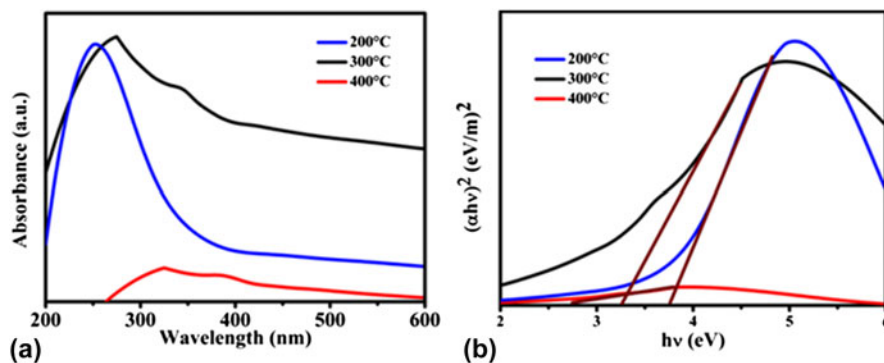

FIG. 2. (a) UV-visible absorption spectra and (b) band gap energy (E_g) of the NiO NPs at different annealing temperatures.
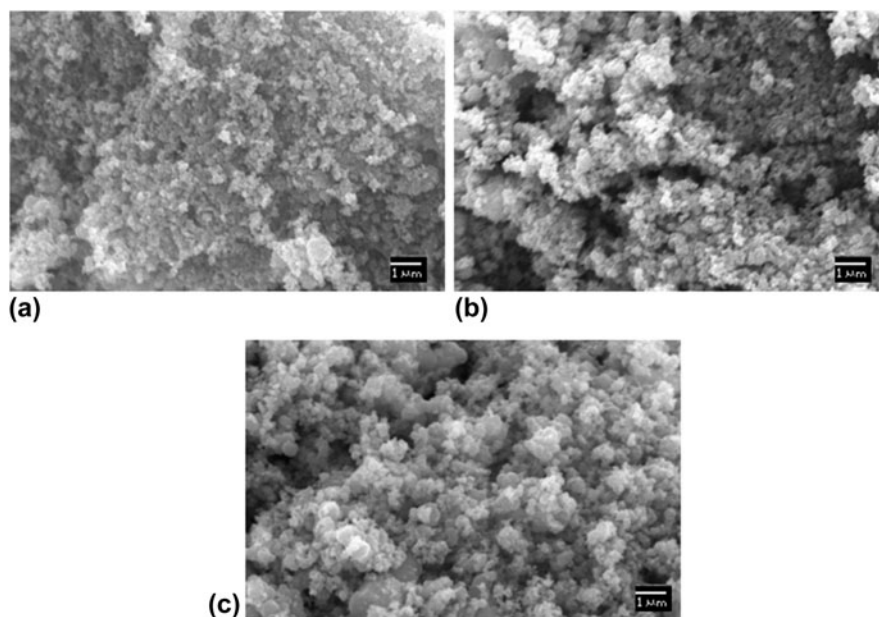
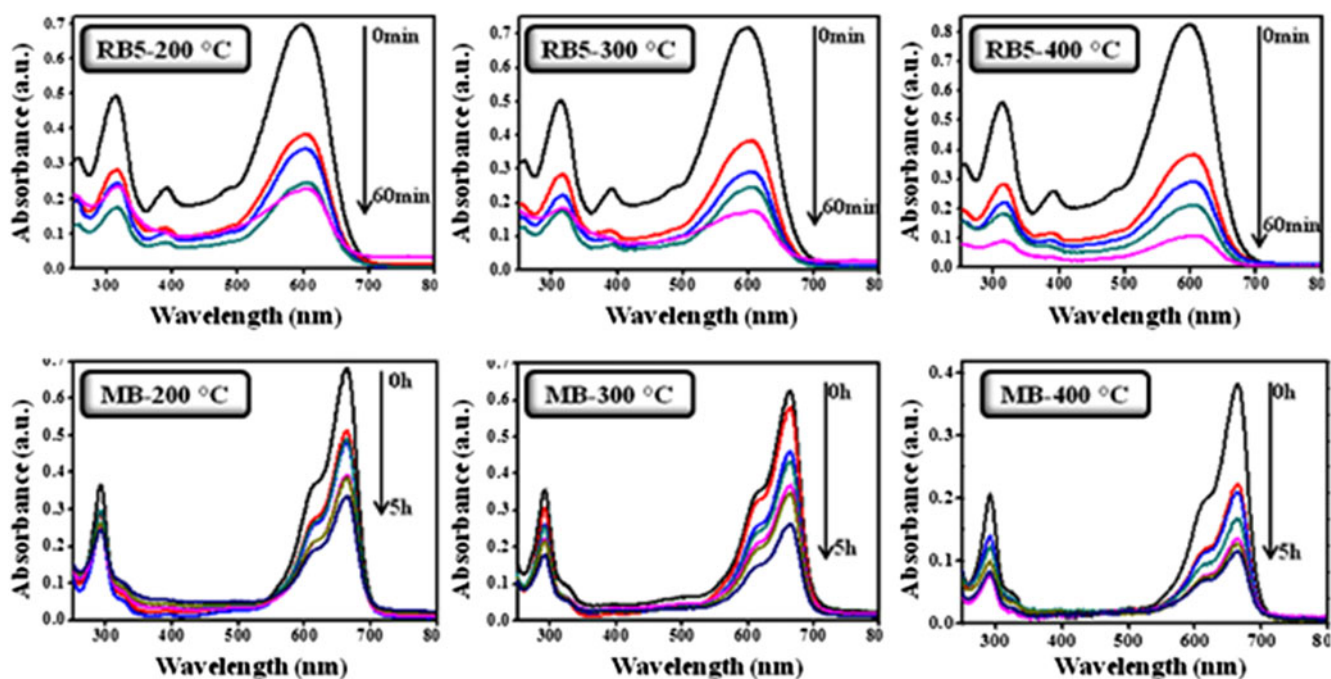FIG. 3. Micrographs of the NiO NPs at different temperatures of (a) 200 °C, (b) 300 °C, and (c) 400 °C.

FIG. 4. UV-visible absorption spectra for the catalysis of RB-5 and MB over NiO NPs annealed at different temperatures of 200 °C, 300 °C, and 400 °C. The concentration of the (RB-5 and MB) dye in the experiment is 30 μM, pH = 5, and dosage of the NiO (0.2 M of NaOH and 0.1 M of NiNO3·6H$_2$O) is 30 mg.

It is to be noted that the intensity of the absorption at the highest peak is directly related to the concentration of dye. Simultaneously, the intensity of maximum absorption peak decreases toward the higher wave length and the color of the solution slightly changes to light gray due to degradation of chromosphere and auxochrome (methyl and methylamine) groups, through the demethylation and hydroxylation process.[17,18] Eventually, a small bond due to the aromatic rings in MB begins to degrade into a monosubstituted molecule; this suggests that the photodegradation not only destroys the conjugate system (–N=N–) but also breaks down partially or totally the intermediate products.[19] These results also indicate that NiO NPs can effectively degrade the MB dye under visible light irradiation.

The dye removal efficiency of NiO NPs toward RB-5 adsorption and photodegradation of MB is calculated from Eq. (3),[20] as shown in Fig. 5. Here, C_0 and C_t are the initial dye concentration and concentration at reaction time t, respectively.

$$\text{Efficiency}(\%) = (C_0/C_t) \times 100 \quad . \tag{3}$$

During initial 30 min, RB-5 dye adsorption on NiO NPs was rapid, in the range 0–72.4%. However, later it was seen to be sluggish due to the adsorption limit, estimated in the range of 64.5–87.2%. The removal of dye is mainly affected by the annealing temperature of the catalyst. The dye RB-5 removal efficiency was estimated to be in the range 65–87.2% when NiO NPs are annealed with a temperature range of 200–400 °C, at the reaction time of 60 min. Table II shows the comparison of removal of RB-5 dye under different laboratory conditions.

In the case of MB adsorption over NiO, the removal of dye is rapid in initial stages due to the availability of vacant surface sites, and after a certain time period, it gets nearly saturated. Therefore, the percentage adsorption of dye did not show any appreciable change with time, when the reaction time was increased from 3 to 5 h. By contrast, the degradation of the MB was about 50.8% and 57.6% for the catalyst at an annealing temperature of 200 °C and 300 °C, respectively. Whereas, the sample

annealed at 400 °C shows highest photocatalytic activity, which reached up to 70.2% after irradiation under visible light. Therefore, it is observed that the degradation rate of MB increases with the increase in annealing temperature of the catalyst. An increase in the annealing temperature of NiO NPs results in the decrease of the band gap of NPs as shown in Fig. 2(b). The reduction in E_g favors stronger electronic interaction between the NiO and MB molecules because of easy charge transfer from the valence band to the conduction band. The reduction in band gap enables easier transfer of charge from the catalyst to the Fermi level of the MB molecules. This, in turn, adsorbs a number of MB molecules to the surface of the catalyst, enhancing the dye degradation efficiency.[26] The maximum color removal efficiency of MB in the present work is relatively better than the reported values, as shown in Table III.

The photocatalytic performance in the semiconductors was in general attributed mainly to the band gap. The calculated energy band gap of NiO is in the range of 3.7–2.7 eV, as given in Table I. Considering the wide band gap of NiO, we can expect that NiO NPs prepared at a low annealing temperature only respond to ultraviolet light. Therefore, the wave length of the light for the generation of charge carriers over the MB–NiO system should be less than 400 nm. However, in the present case, the visible light absorption can be explained using the oxygen species in the catalyst. The temperature creates the intermediate energy band close to the valance band to induce the absorption in the visible region. This was
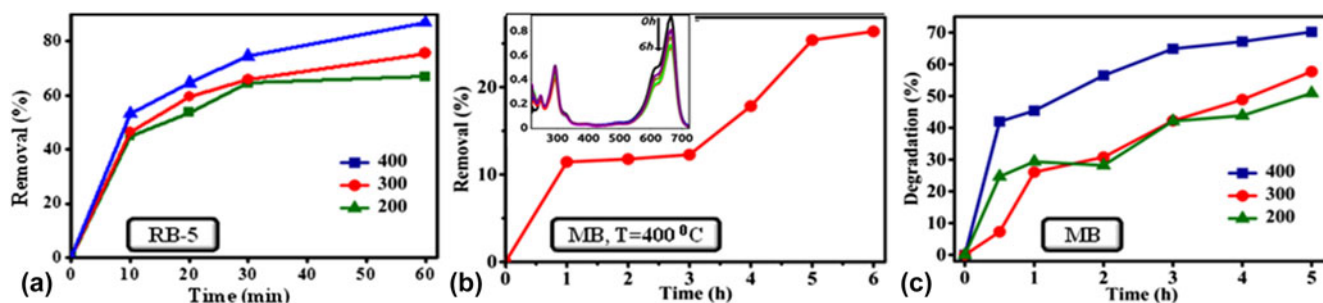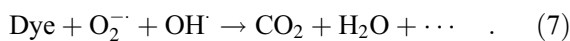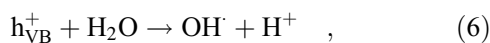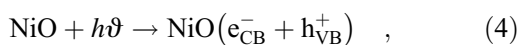

FIG. 5. (a) Effect of annealing temperature of NiO NPs on RB-5 removal efficiency, (b) NiO NPs were tested for the MB removal efficiency (annealing temperature of sample is 400 °C) and the inset of this figure shows UV-visible absorption spectra for the adsorption of MB over NiO NPs in the absence of visible light, and (c) comparative analysis of MB degradation efficiency over NiO NPs in the presence of visible light.

TABLE II. Comparison of RB-5 removal of NiO NPs by adsorption with reported literature values.

Catalyst	Dye concentration	Amount	Source	Time	Removal (%)	Reference
Micrococcus luteus	20 mg/L	. . .	Bio-degradation	3 days	66	21
N-doped TiO_2	10 ppm	0.24 g/200 mL	Visible light	3 (h)	52.4	22
TiO_2	10 mg/L	. . .	UV light	300 (min)	70	23
TiO_2	10 mg/L	. . .	UV light	10 (h)	80	24
CuO	10 ppm	250 mg/L	Ultrasound	60 min	50	25
NiO (200 °C)	3×10^{-5} M	30 mg	No light	60 min	65	Present work
NiO (300 °C)	3×10^{-5} M	30 mg	No light	60 min	70.2	Present work
NiO (400 °C)	3×10^{-5} M	30 mg	No light	60 min	87.2	Present work

ascribed to the formation of oxygen species whose π and π^* molecular orbitals lie just below and above the valence band edge of NiO.[35] The adsorption/catalytic process are associated with removal/degradation efficiency as shown in Fig. 6.

When the NiO NPs in the catalyst system are irradiated by the visible light, the energy absorbed causes an electron to be excited from the valence band to the conduction band. The negatively charged electrons in the conduction band are good reductants, whereas positively charged holes in the valence band are good oxidants [Eq. (4)]. Thereafter, electrons react with atmospheric oxygen to produce superoxide anion radical [Eq. (5)], meanwhile, holes react with water molecules to produce the hydroxyl radicals [Eq. (6)]. These radicals are mainly responsible for the attacking of MB dye molecules, which is adsorbed or close to the surface of NiO NPs [Eq. (7)].[36]

$$NiO + h\vartheta \rightarrow NiO\left(e_{CB}^- + h_{VB}^+\right) \quad , \tag{4}$$

$$e_{CB}^- + O_2 \rightarrow O_2^{-\cdot} \quad , \tag{5}$$

$$h_{VB}^+ + H_2O \rightarrow OH^\cdot + H^+ \quad , \tag{6}$$

$$Dye + O_2^{-\cdot} + OH^\cdot \rightarrow CO_2 + H_2O + \cdots \quad . \tag{7}$$

To examine the details of the process of adsorption and photocatalysis, the kinetics reactions were examined[37]:

$$\mathrm{Log}\, q_e - \frac{k_1 t}{2.303} = \log(q_e - q_t) \quad , \tag{8}$$

$$\frac{t}{q_t} = \frac{1}{k_2 q_e^2} + \frac{t}{q_e} (q_t = 0 \text{ to } q_t = q_e \text{ and } t = 0 \text{ to } t) \quad , \tag{9}$$

where q_t and q_e (both in mg/g) are the quantities of dye adsorbed at time 't' and equilibrium, respectively. K_1 (min^{-1}) and K_2 [g/(mg min)] are the first and second-order rate constants, which can be determined from the slopes by plotting t versus log $(q_e - q_t)$ [Eq. (8)] and t versus t/q_t [Eq. (9)], respectively. For photodegradation, the rate constant was evaluated from t versus $\ln(C_0/C_t)$.

As shown in Fig. 7, all the plots are linear with R^2 (correlation coefficient value), which specified the validity of kinetics. In the adsorption of RB-5 on NiO NPs, the kinetic second-order type has higher R^2 value compared to the first-order type, which indicates that the adsorption process to be a physisorption reaction. The origin of physisorption of the RB-5 was due to the electrostatic interaction between negatively charged sulfonate groups and positively charged shallow donor

TABLE III. Evaluation of photocatalytic degradation of MB dye with reported literature data.

| Catalyst	Dye concentration	Amount	Source	Time (h)	Degradation (%)	Reference
α-Bi$_2$O$_3$ (sol–gel method)	2×10^{-5} M	100 mg	Visible light	6	30	27
α-Bi$_2$O$_3$ (hydrothermal)	2×10^{-5} M	100 mg	Visible light	6	50	‖
Hematite (α-Fe$_2$O$_3$)(0.5%-spheres)	20 mg/L	2.5 g/L	Sun light	8.3	51	28
Hematite (α-Fe$_2$O$_3$)(1% -ellipsoids)	20 mg/L	2.5 g/L	Sun light	8.3	33	‖
CuO (CTAB)	3×10^{-5} M	20 mg	Visible light	6	43	29
HNbWO$_6$	5×10^{-5} M	50 mg	UV light	6	62.5	30
poly(TPT)/TiO$_2$	1×10^{-5} M	40 mg	UV light	7	51.5	31
Flower like CuO	10 mg/L	20 mg	H$_2$O$_2$	8	65	32
ZrO$_2$	20 mg/L	10 mg	UV	2	33	33
ZnS:CdS (wt% 50:50)	10 mg/L	100 mg/L	Visible light	6	65	34
NiO (200 °C)	3×10^{-5} M	30 mg	Visible light	5	50.8	Present work
NiO (300 °C)	3×10^{-5} M	30 mg	Visible light	5	57.7	Present work
NiO (400 °C)	3×10^{-5} M	30 mg	Visible light	5	70.2	Present work
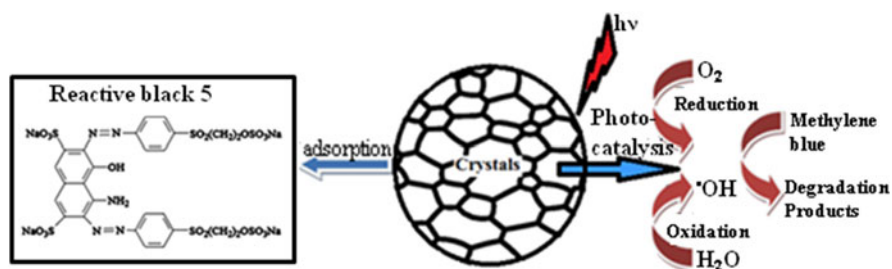
FIG. 6. Schematic representation of the adsorption (left) and photocatalytic process (right) on the surface of NiO NPs using RB-5 dye without irradiation and MB dye with visible light irradiation, respectively.
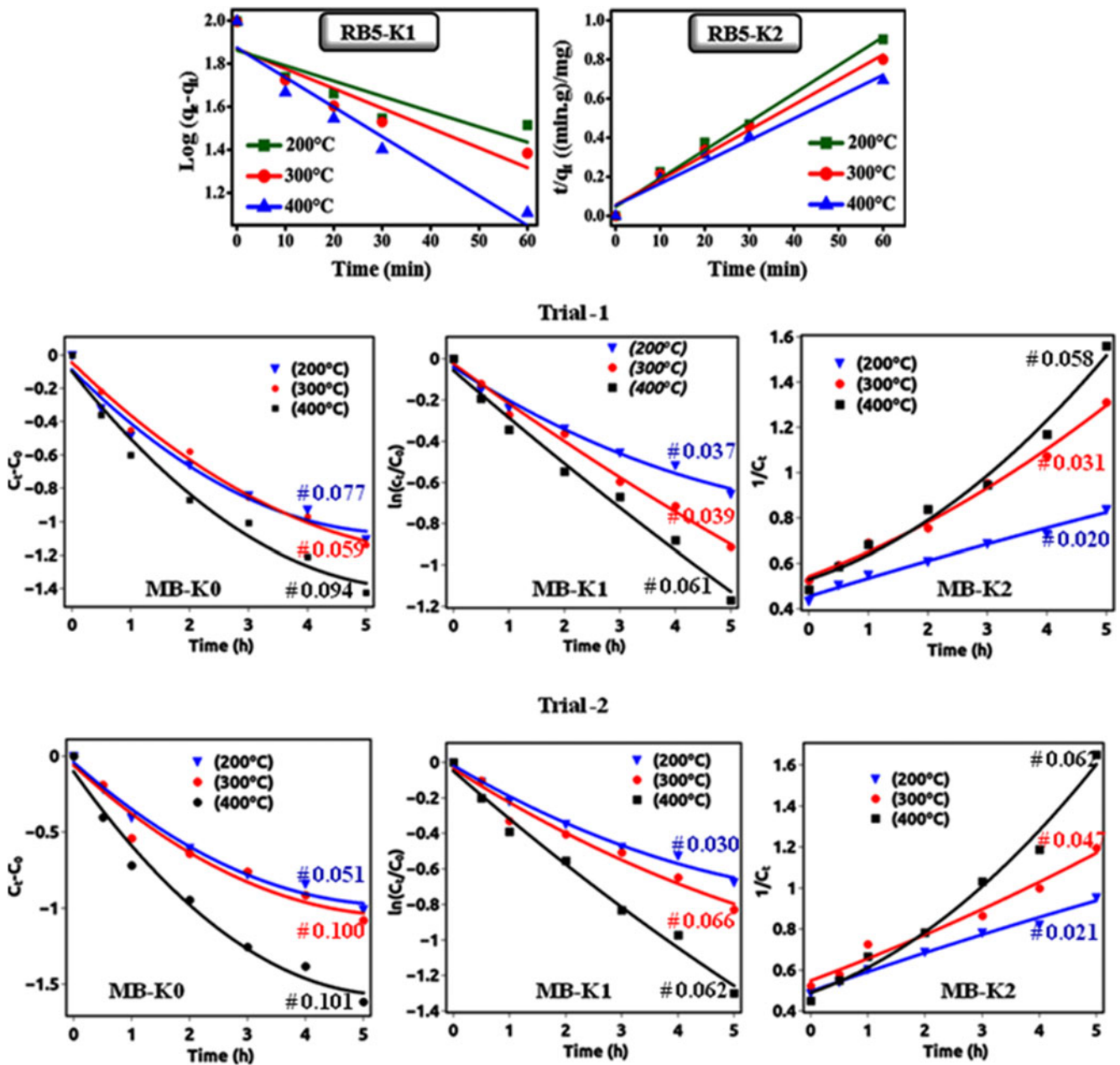
FIG. 7. Shows that the (upper) adsorption follows perfectly the pseudo-second-order kinetic with respect to RB-5 concentrations without irradiation and (lower-trials) photocatalytic degradation follows perfectly the pseudo-first-order kinetic with respect to MB concentrations with irradiation.

defects in the surface region of the NiO NPs. The kinetic values for both graphs are given in Table IV.

For the photodegradation of MB on NiO NPs, the rate constants of the reaction obtained by the polynomial fitting. Polynomial fitting for the particular model estimated using function: $A + Bt + Ct^2$, where A is the zero-order coefficient, B is the first-order coefficient, and C is the second-order coefficient.[38] From Table V, we can conclude that the experimental data fitted well with polynomial regression and first-order model coefficient of determination (R^2) value higher than zero- and second-order models. The

TABLE IV. Kinetic constants for dye RB-5 removal on NiO NPs.

Temp.	First modal		Second modal	
	k_1	R_1^2	k_2	R_2^2
200	0.0071	0.6296	0.0111	0.9847
300	0.0071	0.7875	0.0128	0.9778
400	0.0137	0.9085	0.0144	0.9708

polynomial fitting results revealed that the photocatalytic degradation of MB followed first-order kinetics.

TABLE V. Kinetic constants for dye MB degradation on NiO NPs.

Temp. (°C)	Trial-1				Trial-2			
	A	B (min^{-1})	C (min^{-2})	R^2	A	B (min^{-1})	C (min^{-2})	R^2
$(C_t - C_0) = A + Bt + Ct^2$								
200	−0.216	−0.836	0.035	0.972	−0.531	−0.857	0.046	0.986
300	−0.092	−0.585	0.038	0.980	−0.268	−0.430	0.071	0.954
400	−0.478	−0.299	0.128	0.975	−0.140	−0.050	0.123	0.979
$\ln(C_t/C_0) = A + Bt + Ct^2$								
200	−0.270	−0.566	0.010	0.985	−0.294	−0.531	0.020	0.988
300	−0.093	−0.391	0.019	0.991	−0.144	−0.298	0.037	0.975
400	−0.054	−0.228	0.078	0.984	−0.088	−0.253	0.063	0.987
$1/C_t = A + Bt + Ct^2$								
200	0.473	0.123	−0.047	0.981	0.565	0.142	−0.022	0.987
300	0.546	0.162	−0.016	0.990	0.584	0.176	−0.019	0.973
400	0.629	0.428	0.015	0.983	0.621	0.327	−0.011	0.985

TABLE VI. Comparison of rate constant (k) and correlation coefficient (R^2) values with literature reported values for the removal of dyes.

Catalyst	Dye	k	R^2	Reference
10-ST/BB	Reactive black 5	0.03003	0.94444	39
CeO$_2$/ZnTi–LDH composite	MO	0.0479	0.9615	40
CeO$_2$/ZnTi–LDH composite	MB	0.0429	0.9664	‖
Ir–Sn–Sb oxide	Acid Yellow 36	0.146	0.981	41
α-Fe$_2$O$_3$@GO	MB	0.0190	0.943	42
CO$_3$O$_4$	MB	0.408	95.4	43
TiO$_2$	MB	0.0023	0.942	19
AAc/PVP/ZnO	MB	0.0056	0.961	44
ZnO	RB-5	0.0090	0.9152	45
ZnS	RB-5	0.3477	0.9382	46
NiO	RB-5	0.0144	0.9847	Present work
NiO	MB	0.428	0.995	Present work

As the annealing temperature of the NiO NPs is increased, there is an increment in the rate constant of the kinetic reaction of the dye. This increment in the rate constant is attributed to a reduction in the band gap as well as an increment in the grain size with increase in the annealing temperature. The obtained apparent rate constant values and correlation coefficient (R^2) for the degradation/removal of reactive dyes (MB & RB-5) are found to be higher than the reported values listed in Table VI.

The enhanced adsorption of RB-5 and photocatalytic activity of NiO NPs toward MB can also be explained in terms of surface area. While considering the XRD results, the crystallite size increases with annealing temperature. At higher annealing temperature, the particle possesses a more geometrical surface area due to grain growth. As a result, the particle possesses more catalytically active surface sites, which contribute to the adsorption of more number of dye molecules onto the surface of adsorbent/catalyst.[47]

IV. CONCLUSION

The structural, optical, and adsorption properties of thermally prepared NiO NPs were evaluated. NiO NPs found to be an efficient adsorbent for RB-5 dye molecules

at higher annealing temperature. Evidently, 87.2% of the RB-5 dye was successfully removed within 60 min. It is correlated with the band gap and surface area. Also, RB-5 adsorption on NiO NPs follows second-order kinetics. On the same way, the NiO NPs possess the highest photocatalytic activity at a higher annealing temperature toward the degradation of MB in the presence of visible light. The increment in the degradation efficiency of MB was attributed to the lower band gap of the catalyst. Hence, NiO NPs also can be used as an efficient photocatalyst for degradation of MB from the wastewater. It is established that the annealing temperature of NiO NPs has a significant effect on adsorption/photocatalysis by controlling the particle/grain size. Moreover, these NiO NPs[34] can be used for wastewater treatment technologies.

REFERENCES

1. M.N. Chong, Y.J. Cho, P.E. Poh, and B. Jin: Evaluation of titanium dioxide photocatalytic technology for the treatment of

reactive black 5 dye in synthetic and real greywater effluents. *J. Clean. Prod.* **89**, 196 (2015).

2. J.T. Chacko and K. Subramaniam: Enzymatic degradation of azo dyes—A review. *Int. J. Environ. Sci.* **1**, 1250 (2011).

3. M. Tarrago, M. Garcia-Valles, M.H. Aly, and S. Martínez: Valorization of sludge from a wastewater treatment plant by glass-ceramic production. *Ceram. Int.* **43**, 930 (2017).

4. J. Niu, L. Zhang, Y. Li, J. Zhao, S. Lv, and K. Xiao: Effects of environmental factors on sulfamethoxazole photodegradation under simulated sunlight irradiation: Kinetics and mechanism. *J. Environ. Sci.* **25**, 1098 (2013).

5. E. Kalkan, H. Nadaroğlu, N. Celebi, and G. Tozsin: Removal of textile dye reactive black 5 from aqueous solution by adsorption on laccase-modified silica fume. *Desalin. Water Treat.* **52**, 6122 (2014).

6. J. Vijayaraghavan, S.S. Basha, and J. Jegan: A review on efficacious methods to decolorize reactive azo dye. *J. Urban Environ. Eng.* **7**, 30–47 (2013).

7. M. Farrokhi, S-C. Hosseini, J-K. Yang, and M. Shirzad-Siboni: Application of ZnO–Fe$_3$O$_4$ nanocomposite on the removal of azo dye from aqueous solutions: Kinetics and equilibrium studies. *Water Air Soil Pollut.* **225**, 2113 (2014).

8. M. Ramesh, H.S. Nagaraja, M.P. Rao, S. Anandan, and N.M. Huang: Fabrication, characterization and catalytic activity of α-MnO$_2$ nanowires for dye degradation of reactive black 5. *Mater. Lett.* **172**, 85 (2016).

9. H.J. Song, S. You, X.H. Jia, and J. Yang: MoS$_2$ nanosheets decorated with magnetic Fe$_3$O$_4$ nanoparticles and their ultrafast adsorption for wastewater treatment. *Ceram. Int.* **41**, 13896 (2015).

10. M. El-Kemary, N. Nagy, and I. El-Mehasseb: Nickel oxide nanoparticles: Synthesis and spectral studies of interactions with glucose. *Mater. Sci. Semicond. Process.* **16**, 1747 (2013).

11. N. Murakami, S. Kawakami, T. Tsubota, and T. Ohno: Dependence of photocatalytic activity on particle size of a shape-controlled anatase titanium(IV) oxide nanocrystal. *J. Mol. Catal. Chem.* **358**, 106 (2012).

12. T. Theivasanthi, M. Alagar, and others: Chemical capping synthesis of nickel oxide nanoparticles and their characterizations studies. ArXiv Prepr. *J. Nanosci. Nanotechnol.* **2**, 134–138 (2012).

13. A.G. Al-Sehemi, A.S. Al-Shihri, A. Kalam, G. Du, and T. Ahmad: Microwave synthesis, optical properties and surface area studies of NiO nanoparticles. *J. Mol. Struct.* **1058**, 56 (2014).

14. S-A. Ong, O-M. Min, L-N. Ho, and Y-S. Wong: Comparative study on photocatalytic degradation of mono azo dye acid orange 7 and methyl orange under solar light irradiation. *Water Air Soil Pollut.* **223**, 5483 (2012).

15. A.P. Batista, H.W.P. Carvalho, G.H. Luz, P.F. Martins, M. Gonçalves, and L.C. Oliveira: Preparation of CuO/SiO$_2$ and photocatalytic activity by degradation of methylene blue. *Environ. Chem. Lett.* **8**, 63 (2010).

16. J-H. Sun, S-P. Sun, G-L. Wang, and L-P. Qiao: Degradation of azo dye Amido black 10B in aqueous solution by Fenton oxidation process. *Dyes Pigments* **74**, 647 (2007).

17. M.A. Rauf, M.A. Meetani, A. Khaleel, and A. Ahmed: Photocatalytic degradation of methylene blue using a mixed catalyst and product analysis by LC/MS. *Chem. Eng. J.* **157**, 373 (2010).

18. A. Houas, H. Lachheb, M. Ksibi, E. Elaloui, C. Guillard, and J-M. Herrmann: Photocatalytic degradation pathway of methylene blue in water. *Appl. Catal. B Environ.* **31**, 145 (2001).

19. M.B. Mukhlish, F. Najnin, M.M. Rahman, and M.J. Uddin: Photocatalytic degradation of different dyes using TiO$_2$ with high surface area: A kinetic study. *J. Sci. Res.* **5**, 301 (2013).

20. C. Hachem, F. Bocquillon, O. Zahraa, and M. Bouchy: Decolourization of textile industry wastewater by the photocatalytic degradation process. *Dyes Pigments* **49**, 117 (2001).

21. M.A. Ramdan, A.M. Hashem, W.A. Al-Shareef, and 1.T. Essam: Decolorization of reactive black 5 by micrococcus luteus and Candida albicans in wastewaters. *World Appl. Sci. J.* **32**, 153–163 (2014).

22. N. Kaur, S.K. Shahi, and V. Singh: Anomalous behavior of visible light active TiO$_2$ for the photocatalytic degradation of different reactive dyes. *Photochem. Photobiol. Sci.* **14**, 2024 (2015).

23. T. Kodom, A. Dougna, I. Tchakala, M-E.D. Gnazou, G. Djaneye-Boundjou, and M.L. Bawa: TiO$_2$ PC500 coated on non woven paper with SiO$_2$ as a binder-assisted photocatalytic degradation of reactive black 5 in aqueous solution. *J. Water Resour. Protect.* **5**, 1227 (2013).

24. J. Puentes-Cárdenas, A. Florido-Cuellar, J. Cardona-Bedoya, P. Bohorquez-Echeverry, C. Campos-Pinilla, V. Gutiérrez-Romero, and A. Pedroza-Rodríguez: Simultaneous decolorization and detoxification of black reactive 5 using TiO$_2$ deposited over borosilicate glass. *Univ. Sci.* **17**, 53 (2012).

25. S. Saravanan and T. Sivasankar: Effect of ultrasound power and calcination temperature on the sonochemical synthesis of copper oxide nanoparticles for textile dyes treatment. *Environ. Prog. Sustain. Energy* **25**, 669–679 (2016).

26. S. Fatima, S.I. Ali, M.Z. Iqbal, and S. Rizwan: The high photocatalytic activity and reduced band gap energy of La and Mn co-doped BiFeO$_3$/graphene nanoplatelet (GNP) nanohybrids. *RSC Adv.* **7**, 35928 (2017).

27. M. Jalalah, M. Faisal, H. Bouzid, J-G. Park, S.A. Al-Sayari, and A.A. Ismail: Comparative study on photocatalytic performances of crystalline α- and β-Bi$_2$O$_3$ nanoparticles under visible light. *J. Ind. Eng. Chem.* **30**, 183 (2015).

28. W-F. Tan, Y-T. Yu, M-X. Wang, F. Liu, and L.K. Koopal: Shape evolution synthesis of monodisperse spherical, ellipsoidal, and elongated hematite (α-Fe$_2$O$_3$) nanoparticles using ascorbic acid. *Cryst. Growth Des.* **14**, 157 (2013).

29. M.P. Rao, S. Anandan, S. Suresh, A.M. Asiri, and J.J. Wu: Surfactant assisted synthesis of copper oxide nanoparticles for photocatalytic degradation of methylene blue in the presence of visible light. *Energy Environ. Focus* **4**, 250 (2015).

30. L-F. Hu, R. Li, J. He, L. Da, W. Lv, and J. Hu: Structure and photocatalytic performance of layered HNbWO$_6$ nanosheet aggregation. *J. Nanophotonics* **9**, 093041 (2015).

31. R. Jamal, Y. Osman, A. Rahman, A. Ali, Y. Zhang, and T. Abdiryim: Solid-state synthesis and photocatalytic activity of polyterthiophene derivatives/TiO$_2$ nanocomposites. *Materials* **7**, 3786 (2014).

32. M. Yang and J. He: Fine tuning of the morphology of copper oxide nanostructures and their application in ambient degradation of methylene blue. *J. Colloid Interface Sci.* **355**, 15 (2011).

33. M. Khaksar, M. Amini, D.M. Boghaei, K.H. Chae, and S. Gautam: Mn-doped ZrO$_2$ nanoparticles as an efficient catalyst for green oxidative degradation of methylene blue. *Catal. Commun.* **72**, 1 (2015).

34. N. Soltani, E. Saion, M.Z. Hussein, M. Erfani, A. Abedini, G. Bahmanrokh, M. Navasery, and P. Vaziri: Visible light-induced degradation of methylene blue in the presence of photocatalytic ZnS and CdS nanoparticles. *Int. J. Mol. Sci.* **13**, 12242 (2012).

35. A. Naldoni, M. Allieta, S. Santangelo, M. Marelli, F. Fabbri, S. Cappelli, C.L. Bianchi, R. Psaro, and V. Dal Santo: Effect of nature and location of defects on bandgap narrowing in black TiO$_2$ nanoparticles. *J. Am. Chem. Soc.* **134**, 7600 (2012).

36. A.J. Christy and M. Umadevi: Novel combustion method to prepare octahedral NiO nanoparticles and its photocatalytic activity. *Mater. Res. Bull.* **48**, 4248 (2013).

37. S. Šegota, L. Ćurković, D. Ljubas, V. Svetličić, I.F. Houra, and N. Tomašić: Synthesis, characterization and photocatalytic properties of sol–gel TiO$_2$ films. *Ceram. Int.* **37**, 1153 (2011).

38. D. Lu, P. Fang, W. Wu, J. Ding, L. Jiang, X. Zhao, C. Li, M. Yang, Y. Li, and D. Wang: Solvothermal-assisted synthesis of self-assembling TiO_2 nanorods on large graphitic carbon nitride sheets with their anti-recombination in the photocatalytic removal of Cr(VI) and rhodamine B under visible light irradiation. *Nanoscale* **9**, 3231 (2017).

39. T. Kanagaraj and S. Thiripuranthagan: Photocatalytic activities of novel $SrTiO_3$–BiOBr heterojunction catalysts towards the degradation of reactive dyes. *Appl. Catal. B Environ.* **207**, 218 (2017).

40. S-J. Xia, F-X. Liu, Z-M. Ni, W. Shi, J-L. Xue, and P-P. Qian: Ti-based layered double hydroxides: Efficient photocatalysts for azo dyes degradation under visible light. *Appl. Catal. B Environ.* **144**, 570 (2014).

41. Z.G. Aguilar, E. Brillas, M. Salazar, J.L. Nava, and I. Sirés: Evidence of Fenton-like reaction with active chlorine during the electrocatalytic oxidation of Acid Yellow 36 azo dye with Ir–Sn–Sb oxide anode in the presence of iron ion. *Appl. Catal. B Environ.* **206**, 44–52 (2017).

42. Y. Liu, W. Jin, Y. Zhao, G. Zhang, and W. Zhang: Enhanced catalytic degradation of methylene blue by α-Fe_2O_3/graphene oxide via heterogeneous photo-Fenton reactions. *Appl. Catal. B Environ.* **206**, 642 (2017).

43. G. George and S. Anandhan: Photocatalytic activity of sol–gel electrospun Co_3O_4 nanofibers in degrading methylene blue and methyl orange. Ann mater. *Sci. Eng.* **2**, 1025 (2015).

44. A.E-H. Ali, A.I. Raafat, G.A. Mahmoud, N.A. Badway, M.A. El-Mottaleb, and M.F. Elshahawy: Photocatalytic decolorization of dye effluent using radiation developed polymeric nanocomposites. *J. Inorg. Organomet. Polym. Mater.* **26**, 606 (2016).

45. S. Laohaprapanon, J. Matahum, L. Tayo, and S-J. You: Photodegradation of reactive black 5 in a ZnO/UV slurry membrane reactor. *J. Taiwan Inst. Chem. Eng.* **49**, 136 (2015).

46. E.K. Goharshadi, M. Hadadian, M. Karimi, and H. Azizi-Toupkanloo: Photocatalytic degradation of reactive black 5 azo dye by zinc sulfide quantum dots prepared by a sonochemical method. *Mater. Sci. Semicond. Process.* **16**, 1109 (2013).

47. P. Mehta, R. Mehta, M. Surana, and B.V. Kabra: Influence of operational parameters on degradation of commercial textile azo dye acid blue 113 (cyanine 5r) by advanced oxidation technology. *J. Curr. Chem. Pharm. Sci.* **1**, 28 (2011).